


Synergistic enhancement of spin–phonon interaction in a hybrid system

YUAN ZHOU,^{1,2}  CHANG-SHENG HU,² DONG-YAN LÜ,¹ XIN-KE LI,¹ HAI-MING HUANG,¹ YONG-CHEN XIONG,¹ AND XIN-YOU LÜ^{2,*}

¹School of Mathematics, Physics and Optoelectronic Engineering, Hubei University of Automotive Technology, Shiyan 442002, China

²School of Physics, Huazhong University of Science and Technology, Wuhan 430074, China

*Corresponding author: xinyoulu@hust.edu.cn

Received 7 April 2022; revised 20 May 2022; accepted 21 May 2022; posted 23 May 2022 (Doc. ID 459794); published 30 June 2022

An investigation to significantly enhance coupling to nitrogen–vacancy (NV) centers at a single-quanta level is of great interest to further explore its applications in quantum information processing (QIP). This study explores a joint scheme to further enhance NV–phonon coherent coupling with two methods working together in hybrid optomechanical systems. Both methods are mechanics-induced mode field coupling (MFC) that lead, respectively, to the modification of the spatial distribution of the optical field and the mechanical parametric amplification (MPA) realized by modulating the mechanical spring constant in time. With the joint assistance of MFC and MPA, the coherent coupling between the NV spin and one supermode of the mechanical resonators (MRs) can be further significantly enhanced with the rate $\propto n_{\text{cav}} e^r$. Several potential applications are also discussed in this work. With the ultimate goal to enhance the coupling to NV spin at a single-quanta level, this attempt may provide a promising spin–phonon platform to implement more active control. © 2022 Chinese Laser Press

<https://doi.org/10.1364/PRJ.459794>

1. INTRODUCTION

Implementing a controllable and strong enough coupling to a quantum unit at a single-quanta level is a very desirable basic goal in quantum information processing (QIP) [1–8]. This type of strong coupling can first ensure complete and fast control of the qubits directly or indirectly at the single-quanta level [9,10], which also underlies applications of quantum simulation [11,12], manipulation [13,14], and metrology [15]. Second, such interactions can also be applied to explore many interesting and essential physics [16], such as single photon or phonon technology [17–19] and chiral quantum science [20–22].

Working as a point defect in diamond, the nitrogen–vacancy (NV) center integrated in a hybrid quantum system has recently emerged as one of the leading candidates for QIP. It is desirable thanks to its excellent spin properties [23–26], such as solid-state spins with atom-like properties and without an additional trap device [27,28], precise implantation and easy scalability [29,30], and longer coherence times even at ambient conditions [24,25,31], in addition to the convenient preparation, manipulation, and readout of its quantum state [32,33]. Significant theoretical and experimental investigations have been carried out using NV spins in hybrid systems to realize quantum simulation and quantum state manipulating [34–41]. In recent years, more and more attention has been devoted to the application of NV centers in the quantum acoustics area, which also leads to a growing interest in studying and exploiting

coherent spin–phonon coupling [2,42,43]. However, it is still a huge challenge to significantly enhance the spin–phonon coupling at a single-quanta level by the means currently available [32].

In this work, we present a combined scheme to enhance the spin–phonon coupling in a hybrid setup, which consists of a single NV spin and three optical cavities dispersively coupled with three mechanical resonators (MRs) [44]. To further enhance the spin–phonon coupling in this spin–cavity–resonator tripartite system, there are two key points in our proposal. First, we can modify the spatial distribution of the electric field $\vec{E}(x, y, z)$ in the cavity through mechanical displacement, which is named as the mode field coupling (MFC) [45]. Importantly, the spin–phonon interaction can be controlled and enhanced by the optical field intensity with the rate $\Lambda \propto \vec{E}(x, y, z) \sim \bar{n}_{\text{cav}}$, resulting in optically controlled spin–phonon coherent manipulation. Meanwhile, we apply the mechanical parametric amplification (MPA) to the MR by modulating its spring constant in time [32,46–56]. In the squeezed frame, we can further enhance the spin–phonon coupling with an exponential rate $\Lambda \propto e^r$ in this tripartite system [32,57]. By taking advantage of the joint assistance of MFC and MPA, we have achieved the goal to further strengthen the coherent spin–phonon coupling at a single-quanta level, compared to the previous investigations of this issue. In addition, we also have discussed several potential applications based on

this tripartite interaction system. We believe that this scheme may provide a promising phonon-mediated platform to implement more active control of NV spins.

2. MFC AND MPA

A. MFC

In a traditional cavity quantum electrodynamics (C-QED) system, the realistic dipole coupling to a single quantum emitter (QE) can be written as $g_{\vec{s}} = -\vec{d} \cdot \vec{E}(x, y, z)$, with the emitter's transition dipole moment \vec{d} and the electric field $\vec{E}(x, y, z)$. We note that its coupling strength is determined through a given electric field at the certain position $\vec{r}_0 = (x, y, z)$, and it is impossible to obtain a controllable or enhanced QE–photon coherent coupling in such a system. The MFC can help us to deal with this problem, and its core concept originates from the so-called optomechanical system [44], which indicates that the resonator's displacement $\hat{x} = x_{zpf}(\hat{b} + \hat{b}^\dagger)$ will also affect the cavity frequency $\omega_c(\hat{x}) = \omega_c + \hat{x}\partial\omega_c/\partial\hat{x} + \dots$ with the dispersive coupling $g_0 \approx -(\partial\omega_c/\partial\hat{x})x_{zpf}$. Here, we state x_{zpf} and \hat{b} are, respectively, the zero-point fluctuation and phonon annihilation operator. In addition, we take advantage of the basic idea of the ion trap system, and then we may establish a triple QE–photon–phonon coupled system (namely MFC) that uses the so-called sideband engineering. Importantly, this design will offer a mechanics-induced variation of the spatial distribution of the target cavity field. Going in this direction, we can obtain a mechanic mode-dependent QE–cavity coupling even at the given position and electric field. As a direct consequence, the relevant coupling strength of the QE to cavity mode can be expressed as $g(\hat{x}) = g(0) + \epsilon\hat{x} + \epsilon^2\hat{x}^2/2 + \dots \approx g(0) + \epsilon(\hat{b} + \hat{b}^\dagger)$, where the MFC coupling is defined as $\epsilon = x_{zpf}(\partial g/\partial\hat{x})_{\hat{x}=0}$. With an assumed special condition $g(0) = 0$, we can then get this triple interaction as $\hat{H}_{\text{MFC}} \sim g(\hat{x})(\hat{a}\hat{\sigma}_+ + \text{h.c.}) \approx \epsilon(\hat{b} + \hat{b}^\dagger)(\hat{a}\hat{\sigma}_+ + \hat{a}^\dagger\hat{\sigma}_-)$. When we generally make a classical assumption of this cavity mode with $\hat{a} \approx \alpha \approx \sqrt{n_{\text{cav}}}$, we can obtain an enhanced QE–phonon coupling $\hat{H}_{\text{MFC}} \approx \epsilon\sqrt{n_{\text{cav}}}(\hat{b} + \hat{b}^\dagger)(\hat{\sigma}_+ + \hat{\sigma}_-)$, which results in the MFC-assisted enhancement of the QE–phonon interaction. With the continuous development of the optomechanical technology and applications [58], we have no doubt about the feasibility of this physical mechanism in the future.

We stress that this type of MFC coupling mechanism may be a general proposal, and we can demonstrate it in the traditional optomechanical system and also can introduce it to other optomechanics-like systems; the photon–magnon (lattice) system and the photon–phonon (lattice) system, for example.

B. MPA

Parametric amplification [including optical parametric amplification (OPA) and MPA] has been another hot topic related to the enhancement of coherent coupling since it was first proposed in an optomechanical system. In particular, a milestone achievement on this topic has also been reported and demonstrated in a hybrid ion trap system. This type of progress reinforces our confidence in the feasibility of the OPA or MPA, and we believe that in this work MPA will be a more feasible choice to further enhance the coherent coupling to a single QE. To realize MPA, the core point lies in the modulation of the

time-dependent spring constant [32,50]; i.e., $k = k_0 + \Delta k \cos 2\omega_p t$. Therefore, the Hamiltonian of the mechanical resonator is $\hat{H}_m = \hat{p}^2/2m + k\hat{x}^2/2$, and its quantized expression is $\hat{H}_m = \omega_m \hat{b}^\dagger \hat{b} - \Omega_p (\hat{b}^{\dagger 2} e^{2i\omega_p t} + \hat{b}^2 e^{-2i\omega_p t})/2$. Then, we can transform this mechanical mode into the Bogoliubov mode ($\hat{b} \rightarrow \hat{b}_s^\dagger$ with the squeezing parameter r) and diagonalize this Hamiltonian in a squeezed frame. Next, we can get an exponentially enhanced coupling strength with the expression $\hat{H}_{\text{MFC}} \approx \epsilon e^r \sqrt{n_{\text{cav}}}(\hat{b}_s + \hat{b}_s^\dagger)(\hat{\sigma}_+ + \hat{\sigma}_-)$.

In short, we believe that the MFC and MPA are both general physical ideas, and that this proposal can first show a joint cooperation of the MFC and MPA via a hybrid design to further enhance the EQ–phonon coupling. To induce this joint enhancement effect of the spin–phonon coupling to a feasible hybrid quantum system, we believe that optomechanics [44,58] or an optomechanics-like system will be a suitable choice; for example, the lattice of a photon–phonon coupling system or a hybrid optics–acoustics system [35,59–67]. Here, let's consider the traditional optomechanical system and then discuss this joint scheme in detail.

3. POTENTIAL SCHEME FOR THE JOINT MFC AND MPA

We have designed this hybrid setup, as illustrated in Fig. 1(a), with three identical optical cavities with frequency ω_c arranged one by one, and these optical modes are named, respectively, modes \hat{a}_L , \hat{a}_T , and \hat{a}_R . The central cavity is symmetrically

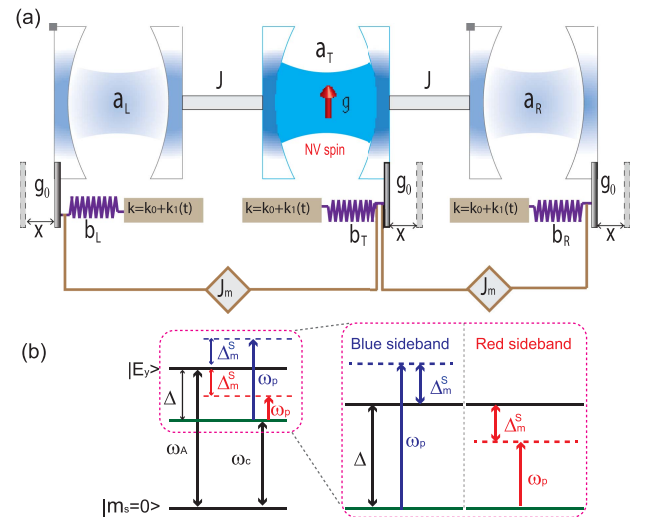


Fig. 1. Schematic of our hybrid system. (a) Three identical optical cavities with frequency ω_c are arranged in a row, and the central cavity couples to the left cavity and the right cavity with the identical coupling strength J , through exchanging photons via optical fibers [68]. Each cavity dispersively couples to the corresponding MR with a coupling strength g_0 . The additional second-order nonlinear pump is applied to each MR, which can be realized by modulating the spring constant in time. The central mechanical resonator is additionally coupled to the other two bilateral MRs with the same coupling rate J_m . A single NV center is placed inside the central cavity and interacts with this cavity mode with the coupling strength g . (b) Energy-level diagram illustrating the blue and red sideband transitions for the tripartite interaction quantum system.

connected to the two bilateral cavities with identical optical fibers. Thus, through the exchange–photon process, the central cavity mode \hat{a}_T will interact with the two bilateral cavities with the same coupling rate J . Each cavity also dispersively couples to an identical MR with the same coupling rate g_0 . For these three identical MRs, the fundamental frequencies are all ω_m , and these mechanical modes are correspondingly named \hat{b}_L , \hat{b}_T , and \hat{b}_R . Moreover, we add an additional second-order nonlinear pump on each resonator, which can be implemented easily through modulation of the mechanical spring constant in time. The central MR \hat{b}_T additionally couples to the other two bilateral MRs \hat{b}_L and \hat{b}_R with the same coupling rate J_m . The coupling between the two mechanical modes can actually be realized by the Coulomb interaction between the charged mechanical media [69,70].

In addition, as illustrated in Fig. 1(a), a single NV center is placed inside the central cavity. In the optical frequency domain, the optical mode \hat{a}_T will induce the NV spin's quantum transition between the excited state $|E_y\rangle$ and the ground state $|m_s = 0\rangle$ with a coupling rate g . The energy level structure of a single NV center is shown in Fig. 1(b). The ground state and the excited state are denoted as $|m_s = 0\rangle \equiv |0\rangle$ and $|E_y\rangle \equiv |1\rangle$, and the optical transition frequency between them is $\omega_A \sim 2\pi \times 470$ THz. For a single NV center, this two-level system $\{|0\rangle, |1\rangle\}$ can be considered as a spin-1/2 particle with Pauli matrix definitions $\hat{\sigma}_z \equiv (|1\rangle\langle 1| - |0\rangle\langle 0|)/2$, $\hat{\sigma}_+ \equiv |1\rangle\langle 0|$, and $\hat{\sigma}_- \equiv |0\rangle\langle 1|$.

Therefore, according to the Appendices A–C, we can get the total Hamiltonian to describe this hybrid system ($\hbar = 1$) by

$$\hat{H}_{\text{Total}} = \hat{H}_1 + \hat{H}_2 + \hat{H}_3, \quad (1)$$

where

$$\begin{aligned} \hat{H}_1 &= \sum_{j=L,R,T} \left[\Delta_m \hat{b}_j^\dagger \hat{b}_j - \frac{\Omega_p}{2} (\hat{b}_j^2 + \hat{b}_j^{\dagger 2}) \right] \\ &\quad + J_m \hat{b}_T^\dagger (\hat{b}_L + \hat{b}_R) + \text{h.c.}, \\ \hat{H}_2 &= \sum_{j=L,R,T} \omega_c \hat{a}_j^\dagger \hat{a}_j + \omega_A \hat{\sigma}_z + g \hat{a}_T^\dagger \hat{\sigma}_- + J \hat{a}_T^\dagger (\hat{a}_L + \hat{a}_R) + \text{h.c.}, \\ \hat{H}_3 &= \sum_{j=L,R,T} [-g_0 \hat{a}_j^\dagger \hat{a}_j (\hat{b}_j^\dagger \exp i\omega_p t + \text{h.c.})]. \end{aligned}$$

In Eq. (1), under the rotating frame with frequency ω_p , the first item \hat{H}_1 is the Hamiltonian to describe these three MRs with the second-order nonlinear interaction, including their pairwise interactions between the central mode \hat{b}_T and the bilateral modes $\hat{b}_{R,L}$. The second item \hat{H}_2 describes the NV spin and optical cavities, with the spin–cavity interaction and the pairwise interactions between the central mode \hat{a}_T and the bilateral modes $\hat{a}_{R,L}$. The last item \hat{H}_3 means the Hamiltonian to describe the dispersive interactions between the cavities and the corresponding mechanical resonators.

According to Appendix D, we can simplify the total Hamiltonian for this system, and obtain an effective Hamiltonian with the tripartite interactions (spin–photon–phonon):

$$\hat{H}_{\text{eff}} \approx \Delta \hat{\sigma}_z + \Delta_m^S \hat{b}_0^\dagger \hat{b}_0 + \frac{g g_0^S}{2J} (\hat{b}_0 + \hat{b}_0^\dagger) (\hat{a}_0^\dagger \hat{\sigma}_- + \text{h.c.}). \quad (2)$$

In view of this Hamiltonian in the squeezed frame, its effective triple coupling strength is strengthened with the rate $e^r/2$ via the MPA process. We also believe this type of enhanced three-body interaction is very important and interesting, especially for the application of QIP, quantum simulation, and quantum manipulation [71–76].

4. ENHANCING THE SPIN–PHONON COUPLING

We consider that the cavity is pumped with a large coherent field with an average photon number $\bar{n}_{\text{cav}} \equiv \sqrt{n_{\text{cav}}}$. Therefore, we can write the cavity field as $\hat{a}_0 = \bar{n}_{\text{cav}} + \delta \hat{a}_0$. Neglecting the quantum fluctuations $\delta \hat{a}_0$ (valid for $n_{\text{cav}} \gg 1$), we can acquire the effective Rabi type Hamiltonian

$$\hat{H}_{\text{eff}} \simeq \Delta \hat{\sigma}_z + \Delta_m^S \hat{b}_0^\dagger \hat{b}_0 + \frac{\bar{n}_{\text{cav}} g g_0^S}{2J} (\hat{b}_0 + \hat{b}_0^\dagger) \hat{\sigma}_x. \quad (3)$$

Next, in the interaction picture (IP), we transfer Eq. (3) into an equivalent expression with the relations $g_0^S = g_0 e^r \cos \omega_p t$ and $\omega_p = \Delta - \Delta_m^S$ (the red sideband detuning), by discarding the high frequency oscillation terms:

$$\hat{H}_{\text{JC}}^{\text{IP}} \simeq \Lambda (\hat{b}_0 \hat{\sigma}_+ + \hat{b}_0^\dagger \hat{\sigma}_-), \quad (4)$$

and this is a Jaynes–Cumming (J–C) type Hamiltonian. On the contrary, when we assume $\omega_p = \Delta + \Delta_m^S$ (the blue sideband detuning), we can also achieve the anti J–C model,

$$\hat{H}_{\text{A-JC}}^{\text{IP}} \simeq \Lambda (\hat{b}_0 \hat{\sigma}_- + \hat{b}_0^\dagger \hat{\sigma}_+). \quad (5)$$

Whether it is a J–C model or an anti J–C model, we can get an enhanced coupling strength with the effective coupling strength

$$\Lambda \equiv \frac{\bar{n}_{\text{cav}} g g_0 e^r}{4J}. \quad (6)$$

To enhance the coherent coupling Λ between the NV spin and supermode \hat{b}_0 , the cooperation of the MFC and MFA is superior to the MFC. This is due to the fact that $\bar{n}_{\text{cav}} \propto \sqrt{P}$ is limited to the driving power P , which can not be increased arbitrarily in a real experiment. For a single NV center, we can achieve a traditional weak spin–phonon coupling at single quantum level with the strength $\lambda/2\pi \leq 0.1$ MHz. To quantify the enhancement of the spin–phonon coupling, we exploit the cooperativity $C = \Lambda^2/\Gamma_m \gamma$. Here, $\Gamma_m = n_{\text{th}} \kappa_m$ and γ correspond, respectively, to the effective mechanical dissipation rates and the decay rate of the spin. Note that in presence of the mechanical amplification, the noise coming from the mechanical bath is also amplified. To circumvent this detrimental effect, a possible strategy is to use the dissipative squeezing approach to keep the mechanical mode in its ground state in the squeezed frame [49,51,77,78]. This steady-state technique has already been implemented experimentally [79]. In this case, we can obtain the engineered effective dissipation rate Γ_m^S in the squeezed frame. Therefore, we can also define the effective cooperativity $C = \Lambda^2/\Gamma_m^S \gamma$.

In Fig. 2, we plot the spin–phonon coupling enhancement Λ/λ and the cooperativity enhancement C , versus the squeeze-

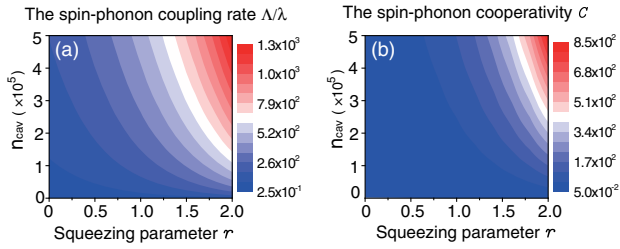


Fig. 2. (a) Spin–phonon coupling enhancement Λ/λ and (b) cooperativity enhancement C versus the squeezing parameter r and the photon number n_{cav} of the cavity mode \hat{a}_0 , with $g_0 = 0.001g$, $J = 10g$, $\lambda/2\pi = 0.1$ MHz, $g/2\pi = 1$ GHz, the effective mechanical dissipation $\Gamma_m^S/2\pi \sim 1$ MHz, and the NV spin decay rate $\gamma/2\pi \sim 15$ MHz.

ing parameter r and photon number n_{cav} of the classical driven field on the mode \hat{a}_0 . Increasing the squeezing parameter r and the photon number n_{cav} , one can achieve a distinct enhancement in the spin–phonon coupling, thus directly giving rise to the cooperativity enhancement.

Furthermore, in Fig. 3, we also plot the dynamical population of the phonon number operator $\hat{b}_0^\dagger \hat{b}_0$ and the spin operator $\hat{\sigma}_z$ according to the J–C model [in Eq. (4)] and the anti J–C model [in Eq. (5)], with the different parameters, such as n_{cav} and r . The numerical results above show the distinct quantum dynamics of this spin–phonon system for different cases, in which the spring constant is modulated or not, and n_{cav} is increased from 5×10^2 to 5×10^4 . Therefore, with the joint assistance of the mechanical squeezing (with parameter r) and the classical driving of the mode \hat{a}_0 (with intensity n_{cav}), the system can be pumped and driven from the weak-coupling regime to the strong-coupling regime, or even to the ultrastrong-coupling regime.

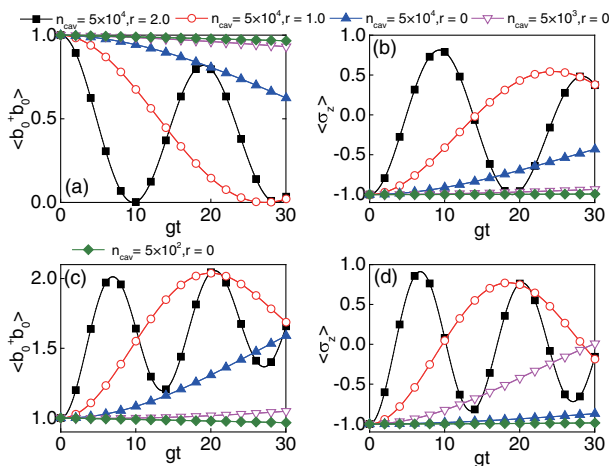


Fig. 3. Dynamical population of the phonon number $\hat{b}_0^\dagger \hat{b}_0$ and the spin operator $\hat{\sigma}_z$ according to (a), (b) the J–C model and (c), (d) the anti J–C model, with different n_{cav} and r . The parameters are $g_0 = 0.001g$ and $J = 10g$, the effective mechanical dissipation is $\Gamma_m^S \sim 0.001\gamma$, and the NV spin decay rate is $\gamma \sim 0.02g$. This system is initially prepared in state $|\phi(0)\rangle = |1\rangle_m |0\rangle_s$.

5. ENHANCEMENT OF PHOTON–SPIN–PHONON INTERACTION

On the other hand, if \bar{n}_{cav} is too weak, the quantum fluctuation $\delta\hat{a}_0$ will dominate the supermode \hat{a}_0 . As a result, we can get the effective tripartite interaction Hamiltonian from Eq. (2) with two different kinds of expression in IP. For the first condition, such as the blue sideband, when the resonance condition satisfies $\omega_p = \Delta + \Delta_m^S$, we can also discard the high frequency oscillation terms, and get the blue sideband effective three-quantum-system Hamiltonian,

$$\hat{H}_{\text{Blue}}^{\text{IP}} \simeq \Lambda_0 (\hat{\sigma}_- \hat{b}_0^\dagger \hat{a}_0^\dagger + \hat{\sigma}_+ \hat{b}_0^\dagger \hat{a}_0). \quad (7)$$

For the second case, such as the red sideband, when the resonance condition satisfies $\omega_p = \Delta - \Delta_m^S$, discarding the high frequency oscillation terms, we can get

$$\hat{H}_{\text{Red}}^{\text{IP}} \simeq \Lambda_0 (\hat{\sigma}_- \hat{b}_0^\dagger \hat{a}_0^\dagger + \hat{\sigma}_+ \hat{b}_0 \hat{a}_0). \quad (8)$$

In this tripartite interaction quantum system, the effective coupling strength is

$$\Lambda_0 = \frac{gg_0 e^r}{4J}. \quad (9)$$

In Fig. 4, we make the simulations on this tripartite interaction system according to Eq. (7) and Eq. (8), and then plot the dynamical population of the phonon number operator

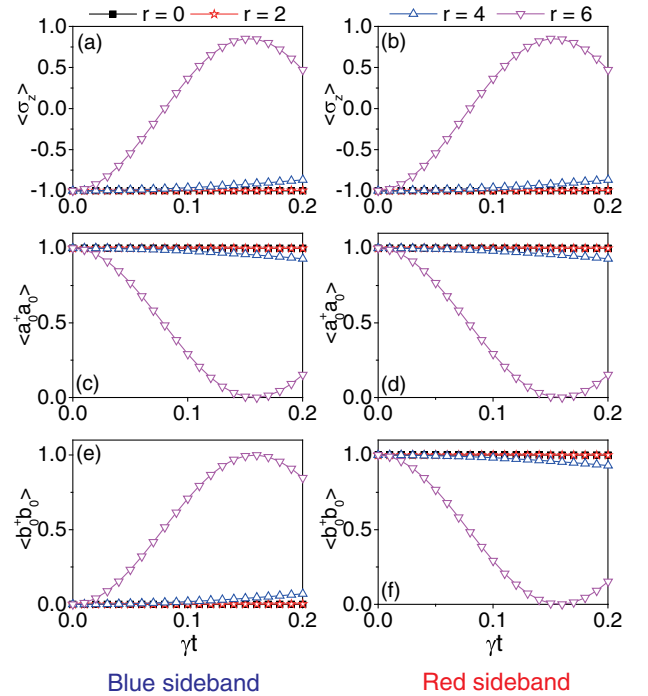


Fig. 4. (a), (b) Dynamical population of the spin operator $\hat{\sigma}_z$, number operators of (c), (d) the optical mode $\hat{a}_0^\dagger \hat{a}_0$ and (e), (f) the phonon mode $\hat{b}_0^\dagger \hat{b}_0$. (a), (c), and (e) correspond to the blue sideband condition, and (b), (d), and (f) correspond to the red sideband condition, with different squeezing parameter r . The parameters are $g_0 \sim \gamma$, $J = 2.8 \times 10^3 \gamma$, and $g \sim 70\gamma$, the effective mechanical dissipation and the cavity decay rate are assumed to be $\Gamma_m^S \sim 0.001\gamma$ and $\kappa \sim 0.1\gamma$, and the NV spin decay rate is $\gamma/2\pi \sim 15$ MHz. This tripartite system is initially prepared, respectively, in states $|\psi(0)\rangle = |1\rangle_o |0\rangle_m |0\rangle_s$ (blue sideband) and $|\psi(0)\rangle = |1\rangle_o |1\rangle_m |0\rangle_s$ (red sideband).

$\hat{b}_0^\dagger \hat{b}_0$, the photon number operator $\hat{a}_0^\dagger \hat{a}_0$, and the spin operator $\hat{\sigma}_z$ with the different squeezing parameter r . The numerical results above evidently show that we can strengthen this tripartite interaction by increasing the squeezing parameter r .

6. APPLICATION OF THIS PROPOSAL

A. Entangling Collective NV Spins Dynamically

In this section, the first potential application for this proposal is that we can entangle separated NV spins. We assume a certain number of NV spins are set separately in this central optical cavity. According to Eq. (3), we can obtain the effective Hamiltonian as

$$\hat{H}_{\text{eff}} \simeq \Delta_m^S \hat{b}_0^\dagger \hat{b}_0 + \sum_k \Lambda^k (\hat{b}_0 + \hat{b}_0^\dagger) \hat{\sigma}_x^k. \quad (10)$$

Here, we assume $\Delta = \omega_A - \omega_c = 0$, and the effective coupling to the k th NV spin is $\Lambda^k = \tilde{n}_{\text{cav}}^k g^k g_0 e^r / 4J$. We stress that this inhomogeneous coupling strength is mainly caused by the differences in the location of NV spins in the cavity, which maps to the factors \tilde{n}_{cav}^k and g^k . In this scheme, one can reduce this system disorder through implanting NV spins precisely with the advanced processing techniques. By discarding this weak adverse effect, we can rewrite the effective Hamiltonian in the interaction picture (IP) as

$$\hat{H}_{\text{eff}}^{\text{IP}} \simeq \Lambda (\hat{b}_0 e^{-i\Delta_m^S t} + \hat{b}_0^\dagger e^{i\Delta_m^S t}) \hat{J}_x. \quad (11)$$

Here, the coupling is identical $\Lambda^k \equiv \Lambda$; therefore, we can use the collective spin operator in the equation above with the definition $\hat{J}_x \equiv \sum_k \hat{\sigma}_x^k$. We note that this type interaction corresponds to the so-called Mølmer–Sørensen (MS) gate [80,81], which is used to generate the multiparticle entanglement. Its system dynamics is governed by the unitary evolution operator $\hat{U}_{\text{IP}}(t) = \exp(-i\hat{H}_{\text{eff}}^{\text{IP}} t)$. Taking advantage of the Magnus formula [82], we get $\hat{U}_{\text{IP}}(\tau) \simeq \exp(-i\Lambda^2 \hat{J}_x^2 \tau / \Delta_m^S)$ when $\tau = 2n\pi / \Delta_m^S$ for the integer number n . This means that the mechanical mode is decoupled from the NV spins at this moment.

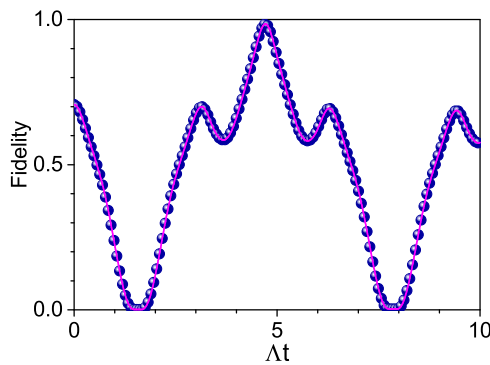


Fig. 5. Dynamical fidelity of the target entangled GHZ state for four NV spins, in which, the initial state is $|\psi_{\text{system}}(0)\rangle = |0\rangle_m |0000\rangle_s$, and the target GHZ state is $|\psi_{\text{r}}^{\text{NV}}\rangle = [e^{-i\pi/4} |0000\rangle_s + e^{i\pi/4} |1111\rangle_s] / \sqrt{2}$. The parameters are the squeezing parameter $r \simeq 4.0$, $g_0 \sim 0.001g$, $J \sim 10g$, $g/2\pi \sim 1.0$ GHz, $\tilde{n}_{\text{cav}} \sim 10^4$, the effective mechanical dissipation $\Gamma_m^S \sim 0.001\gamma$, and the NV spin decay rate $\gamma/2\pi \sim 15$ MHz.

Note that because this operator has no contribution from the mechanical modes, in this instance the system gets insensitive to the states of the mechanical modes. Starting from the initial state of the mechanical mode and NV spins $|\psi_{\text{system}}(0)\rangle = |0\rangle_m |00 \cdots 00\rangle_s$, we can obtain the target entangled state of the collective NV spins with the form $|\psi_{\text{r}}^{\text{NV}}\rangle = [e^{-i\pi/4} |00 \cdots 00\rangle_s + e^{i\pi/4} (-1)^N |11 \cdots 11\rangle_s] / \sqrt{2}$, which is the well-known Greenberger–Horne–Zeilinger (GHZ) type state with N the number of the spins. Next we plot the numerical simulation result shown in Fig. 5. As illustrated in Fig. 5, taking a realistic condition such as the NV decay rate and the mechanical dissipation into consideration, we can quickly entangle NV spins with a high fidelity of more than 0.98 in this scheme.

B. Local Cooling One Supermode of Triple Resonators with an NV Ensemble

On the other hand, we stress that another potential application on this scheme is to cool down the mechanical supermode to its ground state efficiently with the NV center ensemble (NVE). Here, we assume a number of NV centers are set inside the central optical cavity, which form an NVE. Taking the Eqs. (4) and (10) into consideration, we can obtain the effective Hamiltonian in IP for this hybrid system:

$$\hat{H}_{\text{eff}}^{\text{IP}} \simeq \sum_{k=1}^N \Lambda^k (\hat{b}_0 \hat{\sigma}_+^k + \hat{b}_0^\dagger \hat{\sigma}_-^k). \quad (12)$$

Similarly, we can also ignore this weak system disorder adverse effect according to the advanced processing techniques. Then, we can rewrite this effective Hamiltonian as

$$\hat{H}_{\text{eff}}^{\text{IP}} \simeq \Lambda (\hat{b}_0 \hat{J}_+ + \hat{b}_0^\dagger \hat{J}_-), \quad (13)$$

with the collective spin operator $\hat{J}_\pm \equiv \sum_{k=1}^N \hat{\sigma}_\pm^k$. In the condition of weak excitation and $N \gg 1$, we can map the collective spin operators \hat{J}_\mp into the boson operators \hat{d} and \hat{d}^\dagger in the Holstein–Primakoff representation, with $\hat{J}_+ \simeq \sqrt{N} \hat{d}^\dagger$, $\hat{J}_- \simeq \sqrt{N} \hat{d}$, and $\hat{J}_z \simeq (\hat{d}^\dagger \hat{d} - \frac{N}{2})$. Then, we can carry out the goal to efficiently cool down one mechanical supermode

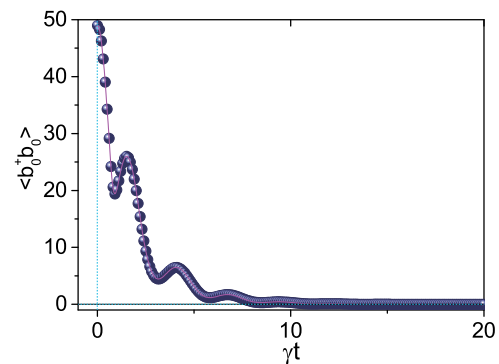


Fig. 6. Dynamical population of this mechanical supermode \hat{b}_0 with the assumption of its initial average phonon number $\langle \hat{b}_0^\dagger \hat{b}_0 \rangle \simeq 50$, in which the parameters are the squeezing parameter $r \simeq 2.0$, $\tilde{n}_{\text{cav}} \sim 100$, $g_0 \sim 0.001g$, $g \sim 66\gamma$, $J \sim 10g$, the effective mechanical dissipation $\Gamma_m^S \sim 0.001\gamma$, and the NV spin decay rate $\gamma/2\pi \sim 15$ MHz.

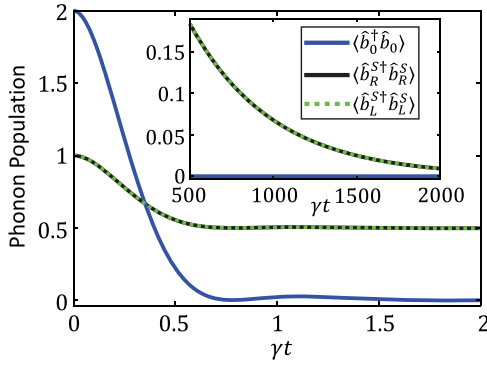


Fig. 7. Dynamical evolution of the mechanical population of the left local mode $\langle \hat{b}_L^\dagger \hat{b}_L^S \rangle$ (green dashed line), the right local mode $\langle \hat{b}_R^\dagger \hat{b}_R^S \rangle$ (black solid line), and the supermode $\langle \hat{b}_0^\dagger \hat{b}_0 \rangle$ (blue solid line) in the time interval $[0, 2/\gamma]$ ($[500/\gamma, 2000/\gamma]$ in the inset), assuming both \hat{b}_R^S and \hat{b}_L^S are initially in the single phonon state. Other parameters are the same as in Fig. 6.

$\hat{b}_0 \equiv (\hat{b}_L^S - \hat{b}_R^S)/\sqrt{2}$ to its ground state. As illustrated in Fig. 6, we can transform this mechanical mode into its quantum ground state completely at the time of $\sim \frac{10}{\gamma}$ through numerically solving the quantum master equation. This result indicates that we can implement this cooling process successfully in this setup. In addition, the two local mechanical modes \hat{b}_L^S and \hat{b}_R^S that consist of the mechanical supermode \hat{b}_0 also can be cooled with the Hamiltonian in Eq. (A3) being realized, as seen in Fig. 7. Compared to the supermode \hat{b}_0 , the local mechanical modes approach their ground state far more slowly. This is due to the spins inducing the generation of the correlation between \hat{b}_L^S and \hat{b}_R^S , which slowly reduces.

7. EXPERIMENTAL PARAMETERS

To examine the feasibility of our scheme in a realistic experiment, we now discuss the relevant experimental parameters. We consider a high-quality optical cavity with frequency $\omega_c/2\pi \sim 470$ THz and $Q \sim 10^6 - 10^8$, and can assume its coupling strength to a single NV center can reach $g/2\pi \sim 10$ GHz [83–89]. For the MR with a frequency $\omega_m/2\pi \sim 1-10$ GHz and $Q \sim 10^5-10^6$, the opto-mechanic coupling to the cavity mode will be $g_0/2\pi \sim 1-10$ MHz [44]. For a single NV center, the lifetime of its excited state is about 10 ns, so the spontaneous decay rate of its excited state is about $\gamma/2\pi \sim 15$ MHz [90–92]. Considering the dynamical process for entangling the NV spins in this work, we can obtain the GHZ state at the time of ~ 0.35 ns. Compared to this time interval, we think its coherence time is enough to implement this scheme.

8. CONCLUSION

In summary, we propose a protocol to further enhance the spin–phonon coupling at the single-quanta level with two methods jointly working together: the MFC and MPA. Importantly, in our scheme, we can enhance the coherent spin–phonon interaction not only by the optical field intensity

with rate $\sim \bar{n}_{\text{cav}}$, but also by the amplified zero-field fluctuation of the mechanical mode with rate $\sim e^r$. In other words, taking advantage of the joint assistance of both amplifications means we can realize the goal to further strengthen the coherent spin–phonon coupling at a single-quanta level in this hybrid system. In addition, we also have to briefly discuss the potential applications of this tripartite interaction system. We believe that this investigation may provide a more promising direction to implement active control of the spin–phonon coupling at a single quanta-level.

APPENDIX A: THE HAMILTONIAN OF MECHANICAL MODES WITH SECOND-ORDER NONLINEAR INTERACTION

The Hamiltonian for the j th mechanical system with a modulated spring constant can be expressed as

$$\hat{H}_{mj} = \frac{\hat{p}_j^2}{2M_j} + \frac{1}{2}k_0\hat{x}_j^2 + \frac{1}{2}k_1(t)\hat{x}_j^2, \quad (\text{A1})$$

where $j = \{R, T, L\}$ and M_j is the effective mass of the j th mechanical resonator. Expressing the momentum operator \hat{p}_j and the displacement operator \hat{x}_j with the oscillator operator \hat{a}_j of the fundamental oscillating mode and the zero field fluctuation $x_{\text{zpf}} = \sqrt{\hbar/2M_j\omega_m}$ [i.e., $\hat{p}_j = -i(M_j\hbar\omega_m/2)^{1/2}(\hat{b}_j - \hat{b}_j^\dagger)$ and $\hat{x}_j = x_{\text{zpf}}(\hat{b}_j^\dagger + \hat{b}_j)$], we obtain ($\hbar = 1$), so

$$\hat{H}_{mj} = \omega_m\hat{b}_j^\dagger\hat{b}_j - \Omega_p \cos 2\omega_p t (\hat{b}_j + \hat{b}_j^\dagger)^2. \quad (\text{A2})$$

Here, we assume that these are three identical MRs, with an intrinsic frequency $\omega_m = \sqrt{k_0/M_j}$, the time-dependent spring constant $k_1(t) = \delta k \cos 2\omega_p t$, and the nonlinear coefficient $-\delta k x_{\text{zpf}}^2/2 \equiv \Omega_p$. Using the frame rotating with frequency ω_p and dropping the terms ($\sim \hat{b}_j^\dagger \hat{b}_j$) that explicitly oscillate in time, then we can acquire the Hamiltonian with a second-order nonlinear interaction for the j th mechanical resonator

$$\hat{H}_{mj} = \Delta_m \hat{b}_j^\dagger \hat{b}_j - \frac{\Omega_p}{2} (\hat{b}_j^2 + \hat{b}_j^{\dagger 2}), \quad (\text{A3})$$

where $\Delta_m = \omega_m - \omega_p$. For simplicity, we assume that Ω_p is a real parameter.

Furthermore, in this scheme, the central mechanical mode \hat{b}_T also interacts with two other bilateral mechanical modes \hat{b}_L and \hat{b}_R . Assuming the identical coupling strength is J_m , we can obtain their Hamiltonian as

$$\begin{aligned} \hat{H}_1 = & \sum_{j=L,R,T} \left[\Delta_m \hat{b}_j^\dagger \hat{b}_j - \frac{\Omega_p}{2} (\hat{b}_j^2 + \hat{b}_j^{\dagger 2}) \right] \\ & + J_m \hat{b}_T^\dagger (\hat{b}_L + \hat{b}_R) + \text{h.c.} \end{aligned} \quad (\text{A4})$$

In this scheme, the coefficient Ω_p of this nonlinear interaction item is tunable using the high precision electromagnetic technology, and the coupling strength J_m between the mechanical modes can also be modulated via some electrical means, such as the capacitor method.

APPENDIX B: THE HAMILTONIAN OF SPIN-CAVITY AND CAVITY-CAVITY INTERACTIONS

As illustrated in Fig. 1(a), a single NV center is set inside the central optical microcavity (mode \hat{a}_T), and this cavity mode will induce the transition between the states $|0\rangle$ and $|1\rangle$. In addition, this cavity also interacts with another two microcavities (modes \hat{a}_L and \hat{a}_R) through exchanging photons. Therefore, we can write the corresponding Hamiltonian in the Schrödinger picture (SP) as

$$\hat{H}_2 = \sum_{j=L,R,T} \omega_c \hat{a}_j^\dagger \hat{a}_j + \omega_A \hat{\sigma}_z + g \hat{a}_T^\dagger \hat{\sigma}_- + J \hat{a}_T^\dagger (\hat{a}_L + \hat{a}_R) + \text{h.c.}, \quad (\text{B1})$$

where ω_c is the fundamental frequency of these three identical cavities, ω_A is the energy-level transition frequency between the ground state $|m_s = 0\rangle$ and the excited state $|E_y\rangle$, and g and J are, respectively, the coupling strength for the spin-cavity interaction and the cavity-cavity interactions.

APPENDIX C: THE INTERACTIONS BETWEEN THE MECHANICAL MODES AND CAVITY MODES

In this scheme, the three cavity modes \hat{a}_j will also interact with the three mechanical modes \hat{b}_j . By setting the same coupling strength as g_0 for simplicity and under the frame rotation with frequency ω_p , we can express this type interaction with the Hamiltonian form,

$$\hat{H}_3 = \sum_{j=L,R,T} \{-g_0 \hat{a}_j^\dagger \hat{a}_j [\hat{b}_j^\dagger \exp(i\omega_p t) + \text{h.c.}]\}, \quad (\text{C1})$$

with the identical dispersive coupling strength g_0 between the cavity modes and the corresponding mechanical modes.

APPENDIX D: THE EFFECTIVE HAMILTONIAN DERIVATION FOR THIS WHOLE SYSTEM

Considering the Hamiltonian in Eq. (1), we can diagonalize the mechanical part of \hat{H}_1 by the unitary transformation $\hat{U}_s(r) = \exp[r(\hat{b}_j^2 - \hat{b}_j^{\dagger 2})/2]$, where the squeezing parameter r is defined via the relation $\tanh 2r = \Omega_p/\Delta_m$. In this squeezed frame, we can obtain the total Hamiltonian with the new expression

$$\hat{H}_{\text{Total}}^S = \hat{H}_1^S + \hat{H}_2^S + \hat{H}_3^S, \quad (\text{D1})$$

where

$$\begin{aligned} \hat{H}_1^S &= \sum_{j=L,R,T} \Delta_m^S \hat{b}_j^{\dagger S} \hat{b}_j^S + J_m^S \hat{b}_T^{\dagger S} (\hat{b}_L^S + \hat{b}_R^S) + \text{h.c.}, \\ \hat{H}_2^S &= \hat{H}_2, \\ \hat{H}_3^S &= \sum_{j=L,R,T} [-g_0^S \hat{a}_j^\dagger \hat{a}_j (\hat{b}_j^{\dagger S} + \hat{b}_j^S)]. \end{aligned}$$

Here, the relevant coefficients are defined, respectively, as

$$\begin{aligned} \alpha &= \Omega_p/\Delta_m, \\ \Delta_m^S &= \Delta_m(1 - \alpha^2)^{1/2}, \\ 4r &= \ln(1 + \alpha)/(1 - \alpha), \\ g_0^S &= g_0 e^r \cos \omega_p t, \\ J_m^S &= J_m e^{2r}/2. \end{aligned} \quad (\text{D2})$$

The mechanical part of this Hamiltonian can also be diagonalized by the canonical transformation

$$\begin{aligned} \hat{b}_T^S &= (\hat{b}_+ - \hat{b}_-)/\sqrt{2}, \\ \hat{b}_L^S &= (\hat{b}_+ + \hat{b}_- + \sqrt{2}\hat{b}_0)/2, \\ \hat{b}_R^S &= (\hat{b}_+ + \hat{b}_- - \sqrt{2}\hat{b}_0)/2, \end{aligned} \quad (\text{D3})$$

where the modes $\hat{b}_{\pm,0}$ are the mechanical supermodes of the resonators. Then, we define the dimensionless position operators of these mechanical supermodes $\hat{x}_0 = \hat{b}_0^\dagger + \hat{b}_0$ and $\hat{x}_\pm = \hat{b}_\pm^\dagger + \hat{b}_\pm$. In addition to the constraint condition $|\Delta_m^S \pm \sqrt{2}J_m^S| \gg |\omega_A - \omega_c|$, we can discard modes \hat{b}_\pm and only focus on the single mode \hat{b}_0 in this system. Then, the Hamiltonian ($\hat{H}_1^S + \hat{H}_3^S$) can be simplified as

$$\hat{H}_1^S + \hat{H}_3^S \simeq \Delta_m^S \hat{b}_0^\dagger \hat{b}_0 + \frac{g_0^S}{\sqrt{2}} \hat{x}_0 (\hat{a}_R^\dagger \hat{a}_R - \hat{a}_L^\dagger \hat{a}_L). \quad (\text{D4})$$

Applying a unitary transformation with the definition $\hat{U} = \exp[-i\omega_c(\hat{a}_L^\dagger \hat{a}_L + \hat{a}_T^\dagger \hat{a}_T + \hat{a}_R^\dagger \hat{a}_R + \hat{\sigma}_z)t]$ to the Hamiltonian \hat{H}_{Total}^S , we can obtain

$$\begin{aligned} \hat{H}_{\text{Total}}^S &= \Delta \hat{\sigma}_z + \Delta_m^S \hat{b}_0^\dagger \hat{b}_0 + \hat{\Theta} (\hat{a}_R^\dagger \hat{a}_R - \hat{a}_L^\dagger \hat{a}_L) + g \hat{a}_T^\dagger \hat{\sigma}_- \\ &+ J \hat{a}_T^\dagger (\hat{a}_L + \hat{a}_R) + \text{h.c.}, \end{aligned} \quad (\text{D5})$$

where $\Delta = \omega_A - \omega_c$ and $\hat{\Theta} = g_0 \hat{x}_0/\sqrt{2}$.

Then, we can also diagonalize the cavity-mode part in the Hamiltonian \hat{H}_{Total}^S by introducing another canonical transformation

$$\begin{aligned} \hat{a}_0 &= -r_1 \hat{a}_L + r_2 \hat{a}_T + r_1 \hat{a}_R, \\ \hat{a}_+ &= r_3 \hat{a}_L - r_1 \hat{a}_T + r_4 \hat{a}_R, \\ \hat{a}_- &= r_4 \hat{a}_L + r_1 \hat{a}_T + r_3 \hat{a}_R, \end{aligned} \quad (\text{D6})$$

where $r_1 = J/E$, $r_2 = \hat{\Theta}/E$, $r_3(\hat{\Theta}, J) = r_4(-\hat{\Theta}, J)$, and $E = \sqrt{2J^2 + \hat{\Theta}^2}$. Then, the Hamiltonian \hat{H}_{Total}^S can also be further simplified as

$$\begin{aligned} \hat{H}_{\text{Total}}^S &= \Delta \hat{\sigma}_z + \Delta_m^S \hat{b}_0^\dagger \hat{b}_0 + E(\hat{a}_+^\dagger \hat{a}_+ - \hat{a}_-^\dagger \hat{a}_-) + g r_2 \hat{a}_0^\dagger \hat{\sigma}_- \\ &+ g r_1 (\hat{a}_+^\dagger - \hat{a}_-^\dagger) \hat{\sigma}_- + \text{h.c.} \end{aligned} \quad (\text{D7})$$

When the spectral separation between the supermodes is much larger than the mechanical frequency ($E \gg \Delta_m^S$), we can neglect the effect of the terms of supermodes \hat{a}_\pm and get the effective Hamiltonian by using the approximate relation $r_2 = \hat{\Theta}/E \approx g_0 \hat{x}_0/2J$ so

$$\hat{H}_{\text{eff}} \approx \Delta \hat{\sigma}_z + \Delta_m^S \hat{b}_0^\dagger \hat{b}_0 + \frac{g g_0^S}{2J} (\hat{b}_0 + \hat{b}_0^\dagger) (\hat{a}_0^\dagger \hat{\sigma}_- + \text{h.c.}) \quad (\text{D8})$$

Funding. National Key Research and Development Program of China (2021YFA1400700); National Natural Science Foundation of China (11774282, 11774285, 11822502, 11875029, 11974125); China Postdoctoral Science Foundation (2021M691150); Natural Science Foundation of Hubei Province (2020CFB748); Natural Science Foundation of Shandong Province (ZR2021MA042, ZR2021MA078); Research Project of Hubei Education Department (B2020078, B2020079, D20201803); Program for Science and Technology Innovation Team in Colleges of Hubei Province (T2021012); Doctoral Scientific Research Foundation of Hubei University of Automotive Technology (HUAT) (BK201906, BK202008, BK202113); Open Fund of HUAT (QCCLSZK2021A07); Foundation of Discipline Innovation Team of HUAT.

Acknowledgment. Yuan Zhou thanks Peng-Bo Li for valuable discussions. Part of the simulations are coded in Python using the QuTiP library [93,94].

Disclosures. The authors declare that there are no conflicts of interest related to this paper.

Data Availability. All relevant data are available from the corresponding author upon request.

REFERENCES

1. A. Imamoglu, D. D. Awschalom, G. Burkard, D. P. DiVincenzo, D. Loss, M. Sherwin, and A. Small, "Quantum information processing using quantum dot spins and cavity QED," *Phys. Rev. Lett.* **83**, 4204–4207 (1999).
2. M. J. A. Schuetz, E. M. Kessler, G. Giedke, L. M. K. Vandersypen, M. D. Lukin, and J. I. Cirac, "Universal quantum transducers based on surface acoustic waves," *Phys. Rev. X* **5**, 031031 (2015).
3. C. Junge, D. O'Shea, J. Volz, and A. Rauschenbeutel, "Strong coupling between single atoms and nontransversal photons," *Phys. Rev. Lett.* **110**, 213604 (2013).
4. Y.-X. Liu, J. Q. You, L. F. Wei, C. P. Sun, and F. Nori, "Optical selection rules and phase-dependent adiabatic state control in a superconducting quantum circuit," *Phys. Rev. Lett.* **95**, 087001 (2005).
5. M. Atatüre, D. Englund, N. Vamivakas, S.-Y. Lee, and J. Wrachtrup, "Material platforms for spin-based photonic quantum technologies," *Nat. Rev. Mater.* **3**, 38–51 (2018).
6. N. Yao, L. Jiang, A. Gorshkov, P. Maurer, G. Giedke, J. Cirac, and M. Lukin, "Scalable architecture for a room temperature solid-state quantum information processor," *Nat. Commun.* **3**, 800 (2012).
7. K. Nemoto, M. Trupke, S. J. Devitt, A. M. Stephens, B. Scharfenberger, K. Buczak, T. Nöbauer, M. S. Everitt, J. Schmiedmayer, and W. J. Munro, "Photonic architecture for scalable quantum information processing in diamond," *Phys. Rev. X* **4**, 031022 (2014).
8. G.-Q. Zhang, Z. Chen, D. Xu, N. Shammah, M. Liao, T.-F. Li, L. Tong, S.-Y. Zhu, F. Nori, and J. Q. You, "Exceptional point and cross-relaxation effect in a hybrid quantum system," *PRX Quantum* **2**, 020307 (2021).
9. T. D. Ladd, F. Jelezko, R. Laflamme, Y. Nakamura, C. Monroe, and J. L. O'Brien, "Quantum computers," *Nature* **464**, 45–53 (2010).
10. L. Buluta and F. Nori, "Quantum simulators," *Science* **326**, 108–111 (2009).
11. I. M. Georgescu, S. Ashhab, and F. Nori, "Quantum simulation," *Rev. Mod. Phys.* **86**, 153–185 (2014).
12. J. Cai, A. Retzker, F. Jelezko, and M. B. Plenio, "A large-scale quantum simulator on a diamond surface at room temperature," *Nat. Phys.* **9**, 168–173 (2013).
13. Z.-L. Xiang, S. Ashhab, J. Q. You, and F. Nori, "Hybrid quantum circuits: superconducting circuits interacting with other quantum systems," *Rev. Mod. Phys.* **85**, 623–653 (2013).
14. M. Wu, A. C. Hryciw, C. Healey, D. P. Lake, H. Jayakumar, M. R. Freeman, J. P. Davis, and P. E. Barclay, "Dissipative and dispersive optomechanics in a nanocavity torque sensor," *Phys. Rev. X* **4**, 021052 (2014).
15. H. Zhou, J. Choi, S. Choi, R. Landig, A. M. Douglas, J. Isoya, F. Jelezko, S. Onoda, H. Sumiya, P. Cappellaro, H. S. Knowles, H. Park, and M. D. Lukin, "Quantum metrology with strongly interacting spin systems," *Phys. Rev. X* **10**, 031003 (2020).
16. M. Mitchell, D. P. Lake, and P. E. Barclay, "Optomechanically amplified wavelength conversion in diamond microcavities," *Optica* **6**, 832–838 (2019).
17. A. Reiserer and G. Remppe, "Cavity-based quantum networks with single atoms and optical photons," *Rev. Mod. Phys.* **87**, 1379–1418 (2015).
18. A. Nunnenkamp, K. Børkje, and S. M. Girvin, "Single-photon optomechanics," *Phys. Rev. Lett.* **107**, 063602 (2011).
19. M. Mitchell, B. Khanaliloo, D. P. Lake, T. Masuda, J. P. Hadden, and P. E. Barclay, "Single-crystal diamond low-dissipation cavity optomechanics," *Optica* **3**, 963–970 (2016).
20. P. Lodahl, S. Mahmoodian, S. Stobbe, A. Rauschenbeutel, P. Schneeweiss, J. Volz, H. Pichler, and P. Zoller, "Chiral quantum optics," *Nature* **541**, 473–480 (2017).
21. I. Söllner, S. Mahmoodian, S. L. Hansen, L. Midolo, A. Javadi, G. Kiršanskė, T. Pregonato, H. El-Ella, E. H. Lee, J. D. Song, S. Stobbe, and P. Lodahl, "Deterministic photon-emitter coupling in chiral photonic circuits," *Nat. Nanotechnol.* **10**, 775 (2015).
22. Y. Zhou, D.-Y. Lü, and W.-Y. Zeng, "Chiral single-photon switch-assisted quantum logic gate with a nitrogen-vacancy center in a hybrid system," *Photon. Res.* **9**, 405–415 (2021).
23. M. W. Doherty, N. B. Manson, P. Delaney, F. Jelezko, J. Wrachtrup, and L. C. L. Hollenberg, "The nitrogen-vacancy colour centre in diamond," *Phys. Rep.* **528**, 1–45 (2013).
24. N. Bar-Gill, L. M. Pham, A. Jarmola, D. Budker, and R. L. Walsworth, "Solid-state electronic spin coherence time approaching one second," *Nat. Commun.* **4**, 1743 (2013).
25. P. Neumann, R. Kolesov, B. Naydenov, J. Beck, F. Rempp, M. Steiner, V. Jacques, G. Balasubramanian, M. L. Markham, and D. J. Twitchen, "Quantum register based on coupled electron spins in a room-temperature solid," *Nat. Phys.* **6**, 249–253 (2010).
26. W. Xiong, J. Chen, B. Fang, M. Wang, L. Ye, and J. Q. You, "Strong tunable spin-spin interaction in a weakly coupled nitrogen vacancy spin-cavity electromechanical system," *Phys. Rev. B* **103**, 174106 (2021).
27. X. Zhu, S. Saito, A. Kemp, K. Kakuyanagi, S. Karimoto, H. Nakano, W. J. Munro, Y. Tokura, M. S. Everitt, and K. Nemoto, "Coherent coupling of a superconducting flux qubit to an electron spin ensemble in diamond," *Nature* **478**, 221–224 (2011).
28. P. E. Barclay, K.-M. C. Fu, C. Santori, A. Faraon, and R. G. Beausoleil, "Hybrid nanocavity resonant enhancement of color center emission in diamond," *Phys. Rev. X* **1**, 011007 (2011).
29. Y. Kubo, F. R. Ong, P. Bertet, D. Vion, V. Jacques, D. Zheng, A. Dréau, J.-F. Roch, A. Auffeves, F. Jelezko, J. Wrachtrup, M. F. Barthe, P. Bergonzo, and D. Esteve, "Strong coupling of a spin ensemble to a superconducting resonator," *Phys. Rev. Lett.* **105**, 140502 (2010).
30. D. Marcos, M. Wubs, J. M. Taylor, R. Aguado, M. D. Lukin, and A. S. Sørensen, "Coupling nitrogen-vacancy centers in diamond to superconducting flux qubits," *Phys. Rev. Lett.* **105**, 210501 (2010).
31. D. A. Golter, T. K. Baldwin, and H. Wang, "Protecting a solid-state spin from decoherence using dressed spin states," *Phys. Rev. Lett.* **113**, 237601 (2014).
32. P.-B. Li, Y. Zhou, W.-B. Gao, and F. Nori, "Enhancing spin-phonon and spin-spin interactions using linear resources in a hybrid quantum system," *Phys. Rev. Lett.* **125**, 153602 (2020).
33. P.-B. Li, Z.-L. Xiang, P. Rabl, and F. Nori, "Hybrid quantum device with nitrogen-vacancy centers in diamond coupled to carbon nanotubes," *Phys. Rev. Lett.* **117**, 015502 (2016).
34. S. D. Bennett, N. Y. Yao, J. Otterbach, P. Zoller, P. Rabl, and M. D. Lukin, "Phonon-induced spin-spin interactions in diamond

- nanostructures: application to spin squeezing,” *Phys. Rev. Lett.* **110**, 156402 (2013).
35. D. A. Golter, T. Oo, M. Amezcua, K. A. Stewart, and H. Wang, “Optomechanical quantum control of a nitrogen-vacancy center in diamond,” *Phys. Rev. Lett.* **116**, 143602 (2016).
 36. J. Teissier, A. Barfuss, P. Appel, E. Neu, and P. Maletinsky, “Strain coupling of a nitrogen-vacancy center spin to a diamond mechanical oscillator,” *Phys. Rev. Lett.* **113**, 020503 (2014).
 37. P.-B. Li, Y.-C. Liu, S.-Y. Gao, Z.-L. Xiang, P. Rabl, Y.-F. Xiao, and F.-L. Li, “Hybrid quantum device based on NV centers in diamond nanomechanical resonators plus superconducting waveguide cavities,” *Phys. Rev. Appl.* **4**, 044003 (2015).
 38. W. L. Yang, Y. Hu, Z. Q. Yin, Z. J. Deng, and M. Feng, “Entanglement of nitrogen-vacancy-center ensembles using transmission line resonators and a superconducting phase qubit,” *Phys. Rev. A* **83**, 022302 (2011).
 39. Y. Zhou, D.-Y. Lü, G.-H. Wang, Y.-H. Fu, M.-Y. He, and H.-T. Ren, “Improvement on the manipulation of a single nitrogen-vacancy spin and microwave photon at single-quantum level,” *Commun. Theor. Phys.* **73**, 065101 (2021).
 40. Y. Zhou, B. Li, X.-X. Li, F.-L. Li, and P.-B. Li, “Preparing multiparticle entangled states of nitrogen-vacancy centers via adiabatic ground-state transitions,” *Phys. Rev. A* **98**, 052346 (2018).
 41. Y. Zhou, S.-L. Ma, B. Li, X.-X. Li, F.-L. Li, and P.-B. Li, “Simulating the Lipkin-Meshkov-Glick model in a hybrid quantum system,” *Phys. Rev. A* **96**, 062333 (2017).
 42. D. A. Golter, T. Oo, M. Amezcua, I. Lekavicius, K. A. Stewart, and H. Wang, “Coupling a surface acoustic wave to an electron spin in diamond via a dark state,” *Phys. Rev. X* **6**, 041060 (2016).
 43. D. A. Golter and H. Wang, “Optically driven Rabi oscillations and adiabatic passage of single electron spins in diamond,” *Phys. Rev. Lett.* **112**, 116403 (2014).
 44. M. Aspelmeyer, T. J. Kippenberg, and F. Marquardt, “Cavity optomechanics,” *Rev. Mod. Phys.* **86**, 1391–1452 (2014).
 45. M. Cotrufo, A. Fiore, and E. Verhagen, “Coherent atom-phonon interaction through mode field coupling in hybrid optomechanical systems,” *Phys. Rev. Lett.* **118**, 133603 (2017).
 46. D. Rugar and P. Grütter, “Mechanical parametric amplification and thermomechanical noise squeezing,” *Phys. Rev. Lett.* **67**, 699–702 (1991).
 47. S. D. Siena, A. D. Lisi, and F. Illuminati, “Quadrature-dependent Bogoliubov transformations and multiphoton squeezed states,” *Phys. Rev. A* **64**, 063803 (2001).
 48. Y. Wu and R. Côté, “Quadrature-dependent Bogoliubov transformations and multiphoton squeezed states,” *Phys. Rev. A* **66**, 025801 (2002).
 49. X.-Y. Lü, Y. Wu, J. R. Johansson, H. Jing, J. Zhang, and F. Nori, “Squeezed optomechanics with phase-matched amplification and dissipation,” *Phys. Rev. Lett.* **114**, 093602 (2015).
 50. A. Szorkovszky, A. C. Doherty, G. I. Harris, and W. P. Bowen, “Mechanical squeezing via parametric amplification and weak measurement,” *Phys. Rev. Lett.* **107**, 213603 (2011).
 51. M.-A. Lemonde, N. Didier, and A. A. Clerk, “Enhanced nonlinear interactions in quantum optomechanics via mechanical amplification,” *Nat. Commun.* **7**, 11338 (2016).
 52. J.-Q. Liao, K. Jacobs, F. Nori, and R. W. Simmonds, “Modulated electromechanics: large enhancements of nonlinearities,” *New J. Phys.* **16**, 072001 (2014).
 53. A. Szorkovszky, A. A. Clerk, A. C. Doherty, and W. P. Bowen, “Mechanical entanglement via detuned parametric amplification,” *New J. Phys.* **16**, 063043 (2014).
 54. C. Leroux, L. C. G. Govia, and A. A. Clerk, “Enhancing cavity quantum electrodynamics via antisqueezing: synthetic ultrastrong coupling,” *Phys. Rev. Lett.* **120**, 093602 (2018).
 55. W. Ge, B. C. Sawyer, J. W. Britton, K. Jacobs, J. J. Bollinger, and M. Foss-Feig, “Trapped ion quantum information processing with squeezed phonons,” *Phys. Rev. Lett.* **122**, 030501 (2019).
 56. W. Qin, A. Miranowicz, P.-B. Li, X.-Y. Lü, J. Q. You, and F. Nori, “Exponentially enhanced light-matter interaction, cooperativities, and steady-state entanglement using parametric amplification,” *Phys. Rev. Lett.* **120**, 093601 (2018).
 57. S. C. Burd, R. Srinivas, H. M. Knaack, W. Ge, A. C. Wilson, D. J. Wineland, D. Leibfried, J. J. Bollinger, D. T. C. Allcock, and D. H. Slichter, “Quantum amplification of boson-mediated interactions,” *Nat. Phys.* **17**, 898–902 (2021).
 58. J. Zhang, B. Peng, S. Kim, F. Monifi, X. Jiang, Y. Li, P. Yu, L. Liu, Y.-X. Liu, A. Alú, and L. Yang, “Optomechanical dissipative solitons,” *Nature* **600**, 75–80 (2021).
 59. V. Fiore, Y. Yang, M. C. Kuzyk, R. Barbour, L. Tian, and H. Wang, “Storing optical information as a mechanical excitation in a silica optomechanical resonator,” *Phys. Rev. Lett.* **107**, 133601 (2011).
 60. X.-L. Dong, P.-B. Li, T. Liu, and F. Nori, “Unconventional quantum sound-matter interactions in spin-optomechanical-crystal hybrid systems,” *Phys. Rev. Lett.* **126**, 203601 (2021).
 61. M. C. Kuzyk and H. Wang, “Scaling phononic quantum networks of solid-state spins with closed mechanical subsystems,” *Phys. Rev. X* **8**, 041027 (2018).
 62. V. Peano, C. Brendel, M. Schmidt, and F. Marquardt, “Topological phases of sound and light,” *Phys. Rev. X* **5**, 031011 (2015).
 63. S. Kim, X. Xu, J. M. Taylor, and G. Bahl, “Dynamically induced robust phonon transport and chiral cooling in an optomechanical system,” *Nat. Commun.* **8**, 205 (2017).
 64. B.-Y. Xie, G.-X. Su, H.-F. Wang, H. Su, X.-P. Shen, P. Zhan, M.-H. Lu, Z.-L. Wang, and Y.-F. Chen, “Visualization of higher-order topological insulating phases in two-dimensional dielectric photonic crystals,” *Phys. Rev. Lett.* **122**, 233903 (2019).
 65. D. Awschalom, “Development of quantum interconnects (QUICS) for next-generation information technologies,” *PRX Quantum* **2**, 017002 (2021).
 66. M. Barra-Burillo, U. Muniain, S. Catalano, M. Autore, F. Casanova, L. E. Hueso, J. Aizpurua, R. Esteban, and R. Hillenbrand, “Microcavity phonon polaritons from the weak to the ultrastrong phonon-photon coupling regime,” *Nat. Commun.* **12**, 6206 (2021).
 67. J. D. Caldwell, L. Lindsay, V. Giannini, I. Vurgaftman, T. L. Reinecke, S. A. Maier, and O. J. Glembocki, “Low-loss, infrared and terahertz nanophotonics using surface phonon polaritons,” *Nanophotonics* **4**, 44–68 (2015).
 68. C. Joshi, J. Larson, M. Jonson, E. Andersson, and P. Öhberg, “Entanglement of distant optomechanical systems,” *Phys. Rev. A* **85**, 033805 (2012).
 69. W. K. Hensinger, D. W. Utami, H.-S. Goan, K. Schwab, C. Monroe, and G. J. Milburn, “Ion trap transducers for quantum electromechanical oscillators,” *Phys. Rev. A* **72**, 041405 (2005).
 70. R.-X. Chen, L.-T. Shen, and S.-B. Zheng, “Dissipation-induced optomechanical entanglement with the assistance of Coulomb interaction,” *Phys. Rev. A* **91**, 022326 (2015).
 71. X.-F. Zhang, Y.-C. Wen, and Y. Yu, “Three-body interactions on a triangular lattice,” *Phys. Rev. B* **83**, 184513 (2011).
 72. A. J. Daley, J. M. Taylor, S. Diehl, M. Baranov, and P. Zoller, “Atomic three-body loss as a dynamical three-body interaction,” *Phys. Rev. Lett.* **102**, 040402 (2009).
 73. K. W. Mahmud, E. Tiesinga, and P. R. Johnson, “Dynamically decoupled three-body interactions with applications to interaction-based quantum metrology,” *Phys. Rev. A* **90**, 041602 (2014).
 74. F. Petziol, M. Sameti, S. Carretta, S. Wimberger, and F. Mintert, “Quantum simulation of three-body interactions in weakly driven quantum systems,” *Phys. Rev. Lett.* **126**, 250504 (2021).
 75. F. K. Malinowski, F. Martins, P. D. Nissen, S. Fallahi, G. C. Gardner, M. J. Manfra, C. M. Marcus, and F. Kuemmeth, “Symmetric operation of the resonant exchange qubit,” *Phys. Rev. B* **96**, 045443 (2017).
 76. V. Srinivasa, J. M. Taylor, and C. Tahan, “Entangling distant resonant exchange qubits via circuit quantum electrodynamics,” *Phys. Rev. B* **94**, 205421 (2016).
 77. C.-G. Liao, X. Shang, H. Xie, and X.-M. Lin, “Dissipation-driven entanglement between two microwave fields in a four-mode hybrid cavity optomechanical system,” *Opt. Express* **30**, 10306–10316 (2022).
 78. A. Kronwald, F. Marquardt, and A. A. Clerk, “Arbitrarily large steady-state bosonic squeezing via dissipation,” *Phys. Rev. A* **88**, 063833 (2013).
 79. E. E. Wollman, C. U. Lei, A. J. Weinstein, J. Suh, A. Kronwald, F. Marquardt, A. A. Clerk, and K. C. Schwab, “Quantum squeezing of motion in a mechanical resonator,” *Science* **349**, 952 (2015).

80. A. Sørensen and K. Mølmer, "Quantum computation with ions in thermal motion," *Phys. Rev. Lett.* **82**, 1971–1974 (1999).
81. A. Sørensen and K. Mølmer, "Entanglement and quantum computation with ions in thermal motion," *Phys. Rev. A* **62**, 022311 (2000).
82. H. Takahashi, P. Nevado, and M. Keller, "Mølmer-Sørensen entangling gate for cavity QED systems," *J. Phys. B* **50**, 195501 (2017).
83. X. Jiang and L. Yang, "Optothermal dynamics in whispering-gallery microresonators," *Light Sci. Appl.* **9**, 24 (2020).
84. L. Wang, C. Wang, J. Wang, F. Bo, M. Zhang, Q. Gong, M. Lončar, and Y.-F. Xiao, "High-Q chaotic lithium niobate microdisk cavity," *Opt. Lett.* **43**, 2917–2920 (2018).
85. R. Wu, J. Zhang, N. Yao, W. Fang, L. Qiao, Z. Chai, J. Lin, and Y. Cheng, "Lithium niobate micro-disk resonators of quality factors above 10^7 ," *Opt. Lett.* **43**, 4116–4119 (2018).
86. Z. Fang, H. Luo, J. Lin, M. Wang, J. Zhang, R. Wu, J. Zhou, W. Chu, T. Lu, and Y. Cheng, "Efficient electro-optical tuning of an optical frequency microcomb on a monolithically integrated high-Q lithium niobate microdisk," *Opt. Lett.* **44**, 5953–5956 (2019).
87. A. Faraon, C. Santori, Z. Huang, V. M. Acosta, and R. G. Beausoleil, "Coupling of nitrogen-vacancy centers to photonic crystal cavities in monocrystalline diamond," *Phys. Rev. Lett.* **109**, 033604 (2012).
88. P. Lodahl, S. Mahmoodian, and S. Stobbe, "Interfacing single photons and single quantum dots with photonic nanostructures," *Rev. Mod. Phys.* **87**, 347–400 (2015).
89. J. C. Lee, D. O. Bracher, S. Cui, K. Ohno, C. A. McLellan, X. Zhang, P. Andrich, B. Alemán, K. J. Russell, A. P. Magyar, I. Aharonovich, A. Bleszynski Jayich, D. Awschalom, and E. L. Hu, "Deterministic coupling of delta-doped nitrogen vacancy centers to a nanobeam photonic crystal cavity," *Appl. Phys. Lett.* **105**, 261101 (2014).
90. A. Khalid, K. Chung, R. Rajasekharan, D. W. Lau, T. J. Karle, B. C. Gibson, and S. Tomljenovic-Hanic, "Lifetime reduction and enhanced emission of single photon color centers in nanodiamond via surrounding refractive index modification," *Sci. Rep.* **5**, 11179 (2015).
91. G. Burkard, V. O. Shkolnikov, and D. D. Awschalom, "Designing a cavity-mediated quantum cphase gate between NV spin qubits in diamond," *Phys. Rev. B* **95**, 205420 (2017).
92. T. Astner, J. Gugler, A. Angerer, S. Wald, S. Putz, N. J. Mauser, M. Trupke, H. Sumiya, S. Onoda, J. Isoya, J. Schmiedmayer, P. Mohn, and J. Majer, "Solid-state electron spin lifetime limited by phononic vacuum modes," *Nat. Mater.* **17**, 313–317 (2018).
93. J. R. Johansson, P. D. Nation, and F. Nori, "QuTiP: an open-source Python framework for the dynamics of open quantum systems," *Comput. Phys. Commun.* **183**, 1760–1772 (2012).
94. J. R. Johansson, P. D. Nation, and F. Nori, "QuTiP 2: a Python framework for the dynamics of open quantum systems," *Comput. Phys. Commun.* **184**, 1234–1240 (2013).